Verification of different peak centroid analysis algorithms based on airborne wind lidar data in support of ESA's Aeolus mission

Benjamin Witschas[(a)], Michael Vaughan[(b)], Oliver Lux[(a)], Christian Lemmerz[(a)], Ines Nikolaus[(c)], and Oliver Reitebuch[(a)]

[(a)] Deutsches Zentrum für Luft- und Raumfahrt e.V. (DLR), Institute of Atmospheric Physics, Oberpfaffenhofen, Germany

[(b)] Optical & Lidar Associates (OLA), Buckinghamshire, HP14 3PF, UK

[(c)]University of Applied Sciences Munich, Munich, Germany

Benjamin.Witschas@dlr.de

Abstract: The Aeolus mission by ESA was operational from August 2018 to July 2023. Aeolus carried the direct-detection Atmospheric LAser Doppler INstrument (ALADIN). To support Aeolus, the ALADIN Airborne Demonstrator (A2D) was developed. Both ALADIN and A2D consist of so-called Rayleigh and Mie channels to measure wind from molecular and particulate backscatter signals, respectively. The Mie channel relies on determining the spatial location of a fringe being imaged on the detector. The accuracy of the retrieved winds depends on the analytic algorithm used for determining the fringe location. In this paper, the performance of two non-linear fit-based algorithms is investigated by applying them to airborne A2D data. For performance validation, the data of a heterodyne-detection wind lidar are used as a reference. In addition, a fast and non-fit-based algorithm relying on a four-pixel intensity ratio approach (R_4) has been developed and yielded similar accuracy, but at a much faster computation time.

1. Introduction

The Aeolus satellite by ESA was launched in August 2018 and completed its mission in April 2023. The satellite reentered Earth's atmosphere on 28 July 2023. Aeolus carried the Atmospheric LAser Doppler INstrument (ALADIN) on a sun-synchronous orbit at about 320 km altitude, providing wind profiles up to 30 km in the stratosphere. Among others, this data improved numerical weather prediction, especially over the Southern Hemisphere, the tropics, and oceans.

To prepare for Aeolus, the ALADIN Airborne Demonstrator (A2D) with similar specifications was developed and has been used in several field campaigns already since the late 2000s. Both ALADIN and A2D use Rayleigh and Mie channels to measure wind from backscatter signals of atmospheric molecules and particles. The Mie channel employs the fringe-imaging technique, relying on a Fizeau spectrometer to form a linear interference pattern (fringe) imaged on the detector. The accuracy of the performed Mie wind measurements hence depends on the quality of the optical system and the algorithm used to determine the fringe location.

Initially, the Mie-core 2 algorithm, which fits a Lorentzian peak to the fringe data, was used for the Aeolus Mie wind retrieval. However, recent studies indicated that a Voigt profile better describes the Mie fringe, leading to an update in the Aeolus L1B processor in 2022. This change aimed to improve the accuracy of the retrieved scattering ratio and potentially the fringe centroid computation. In parallel, a new algorithm, R_4, based on an intensity ratio on four of the 16 detector pixels, was developed to reduce computation time significantly while maintaining the accuracy of the fit-based centroid determination. This is beneficial for large data sets and various spectroscopic applications but also for near real-time calculations as they are requested for commercial heterodyne-detection wind lidar systems.

This paper compares the performance of the Lorentzian-fit, Voigt-fit, and R_4 algorithms using A2D data from an airborne campaign in Iceland in 2019. The algorithms' accuracy and precision are evaluated against a heterodyne-detection 2-µm Doppler wind lidar (DWL) used as a reference. The study's results are crucial for enhancing the Aeolus Mie wind data quality for future reprocessed datasets.

2. The ALADIN airborne demonstrator (A2D)

The A2D has a very similar architecture as ALADIN and thus, represents an ideal test-bed for ALADIN performance investigations. The laser pulses produced by the A2D laser transmitter have an energy of about 60 mJ at a repetition rate of 50 Hz. It employs a 0.2-m telescope, which is oriented at an off-nadir angle of 20°. Furthermore, the A2D is based on a bi-static design. The A2D receiver chain with the Rayleigh and Mie channels is identical to that of ALADIN, except for specific front optics that take care of the different operating altitude ranges of both instruments. In particular, the light back-scattered from the atmosphere gets directed to the Fizeau interferometer after being transmitted to a field stop. The Fizeau interferometer acts as a narrow-band filter with a bandwidth (FWHM) of 83 fm (195 MHz) to analyze the Mie backscattered light frequency shift. It consists of two reflecting plates, separated by 68.5 mm, creating a free spectral range (FSR) of 0.92 fm (2190 MHz) and an effective finesse of 11.2. The plates are tilted by 4.77 µrad and the space between them is evacuated. The Fizeau fringes are imaged onto an accumulation charge-coupled device (ACCD) with 16 x 16 pixels, covering a useful spectral range of 0.69 fm (1577 MHz). The light reflected from the Fizeau interferometer is analyzed in the Rayleigh channel (not further discussed here).

Although the detection scheme for the A2D is similar to the one of ALADIN, the horizontal resolution of the wind data is higher, namely, about 3.6 km for both channels, due to the lower ground speed of the aircraft (≈ 200 m/s) compared to Aeolus (≈ 7200 m/s). A detailed description of the A2D can be found in [1].

3. The AVATAR-I campaign

The AVATAR-I (Aeolus VAlidation Through Airborne lidaRs in Iceland) campaign was one of four airborne Aeolus calibration and validation campaigns performed by the German Aerospace Center (DLR) and took place from September 9 to October 1, 2019, in Keflavik, Iceland. During AVATAR-I, the DLR operated the Falcon aircraft, equipped with both the A2D and the 2-µm DWL used as a reference system. The 2-µm DWL data were primarily used to validate the quality of the Aeolus L2B wind product, while the A2D data helped to optimize Aeolus wind retrieval and calibration procedures. The campaign included 10 Aeolus underflights, covering approximately 8,000 km of the Aeolus measurement track, along with two specific A2D calibration flights. Additional details about the duration of the flights, start and stop times, and the corresponding geolocations of the Aeolus underflights are available in Table 2 of reference [2].

4. Fizeau fringe analysis algorithms

The transmission function of the ALADIN and A2D Fizeau interferometers is not remarkably affected by asymmetry effects and can, to a first approximation, be described by a Lorentzian peak function [3]. In the Aeolus processor, a Lorentzian is used in a downhill simplex fitting algorithm to determine the Fizeau fringe position and width [4] to finally derive the Doppler shift of the narrow-band backscattered light. However, after a more careful analysis of the measured A2D and ALADIN fringes, it turned out that the fringe profile is better described by a Voigt function that is represented as the convolution of a Lorentzian and a Gaussian peak profile. Recently performed wave optic analysis simulations have revealed that an off-axis illumination of the Fizeau interferometer of about 100 µrad with a divergent laser beam (≈ 500 µrad) can explain the observed Voigt shape of the A2D and Aeolus Mie fringes. As shown by a detailed analysis of the spectral performance of the Aeolus Rayleigh channel, such large off-axes angles are realistic and even likely [5]. For an analytical representation of a Voigt profile, the pseudo-Voigt approximation as a linear combination of a Lorentzian and a Gaussian peak function can be used. Careful analysis of Aeolus ground returns demonstrated that the measured fringe is significantly better described by means of the pseudo-Voigt function (for further details refer to [3]).

For the two fit-based approaches, the signal of all 16 detector pixels, obtained after vertical integration of the fringe image, is analyzed. Considering the Fizeau fringe width of about 195 MHz, the main signal is distributed over only a few pixels, whereas the other ones mainly contain noise and an imperfectly corrected background signal originating from solar radiation as well as from the broadband Rayleigh backscatter signal. Typically, four

pixels around the Fizeau fringe center contain about 84% of the overall signal. With this in mind, it was investigated if the determination of the Fizeau fringe position can be improved by exploiting the information of the four pixels with the highest intensity only. This algorithm is less sensitive to the accurate knowledge of the actual fringe profile, which is difficult to measure from space due to the variable Rayleigh signal contribution and the uncertainty of the Fizeau illumination function. In addition, as the Fizeau fringe profile can be assumed to be stable over time, a non-fit-based algorithm can reduce the computation time significantly, which is beneficial for near-real-time applications.

Consequently, a novel algorithm based on an intensity ratio approach was developed. In particular, a response function R_4 that describes the fringe position between two adjacent pixels is calculated according to

$$R_4 = \frac{(I_{p1} + I_{p2}) - (I_{p3} + I_{p4})}{(I_{p2} + I_{p3}) - (I_{p1} + I_{p4})} \qquad (1)$$

where I_{py} is the signal intensity measured at the pixel *y* of the ACCD detector. The lower index of the two neighboring pixels with the highest intensity is defined to be p_2. Thus, $R_4 = 1$ in case the fringe is centered at p_2, $R_4 = 0$ in case the fringe is in between p_2 and p_3, and $R_4 = -1$ in case the fringe is centered at p_3. The fringe positions of these three edge cases are sketched in Fig. 1. In between these extreme cases, the response function R_4 is almost linear and only marginally depending on the actual fringe shape.

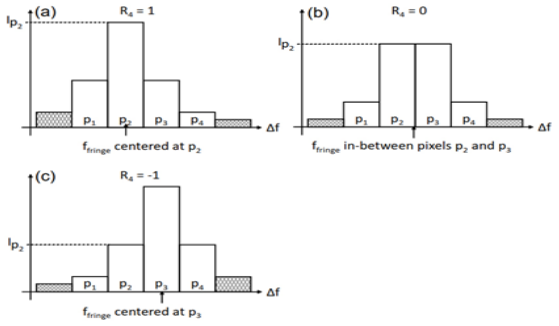

Figure 1. Fizeau fringe intensity distribution for three edge cases having the fringe centered (a) at pixel 2, (b) in between pixel 2 and pixel 3, and (c) at pixel 3, leading to R_4 values of 1, 0, and −1, respectively.

To verify the performance of the R_4 algorithm, simulations with different fringe shapes were performed (FWHM = 150 MHz to 200 MHz). Based on this, it could be demonstrated that the deviation to a line-fit is only about ±0.7 MHz (±0.007 pixels), confirming the insensitivity of the R_4 algorithm to the accurate knowledge of the fringe profile. The deviation to a fifth-order polynomial fit is even smaller (±0.05 MHz). Hence, a fifth-order polynomial, originating from simulation with a certain Voigt profile, is used to describe the relationship between the calculated R_4 value and the actual fringe position between two pixels, as it is needed for the wind retrieval.

5. Algorithm performance validation based on A2D data

The accuracy and precision of the different peak algorithms is investigated by application to A2D Mie data. The retrieved winds are compared to data from the 2-µm DWL reference instrument. Due to the different horizontal and vertical resolutions of both data sets, averaging procedures are applied in advance. The 3D wind vectors measured with the 2-µm DWL were projected onto the single A2D line-of-sight (LOS) axis. Moreover, the 2-µm DWL measurement grid was adapted to that of the A2D by means of a weighted aerial interpolation algorithm. For the analysis, A2D data from all 10 research flights performed during AVATAR-I were analyzed. The corresponding statistical comparison is shown in Figure 2.

The Lorentzian-based algorithm (Figure 2a) provides 5050 valid wind measurements and 180 outliers (3.7%). The determined bias is (0.14 ± 0.02) m/s, and the corresponding random error is 1.50 m/s. The outliers represent a large positive bias for positive LOS winds and a negative bias for negative LOS winds. The root cause for this characteristic is currently unknown. Compared to that, the pseudo-Voigt-based algorithm (Figure 2b) provides 7519 valid wind measurements with 294 outliers (3.9%), corresponding to a considerable gain in data coverage by almost 50%. This result clearly confirms the better performance of the pseudo-Voigt-based algorithm compared to the Lorentzian one. The bias is (−0.39 ± 0.02) m/s and the random error is 1.50 m/s and hence, equally high as for the Lorentzian-based analysis, despite the larger number of valid wind measurements.

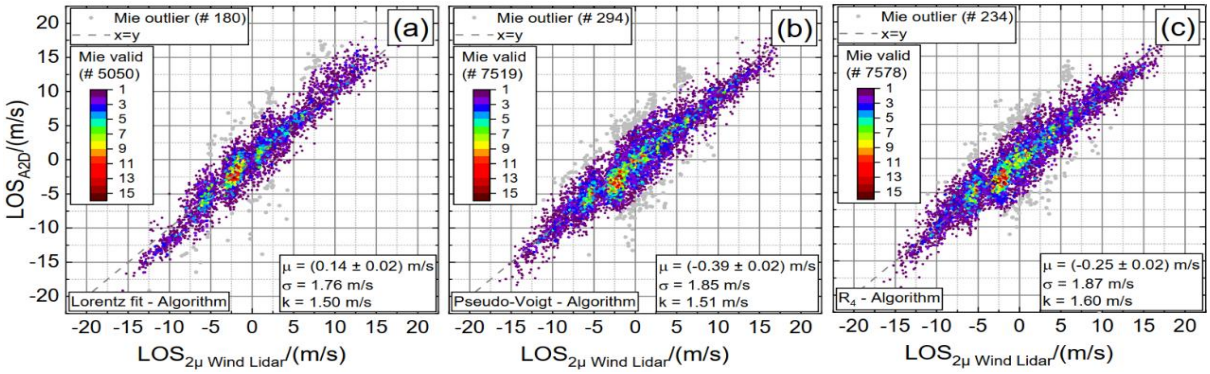

Figure 2. A2D Mie LOS winds plotted against the 2-µm DWL wind speed for all 10 research flights performed during the AVATAR-I campaign, analyzed with the (a) Lorentzian fit algorithm, (b) pseudo-Voigt fit algorithm, and (c) the R_4 algorithm. The color of the points indicates the number of data counts at certain wind speeds. Outliers are indicated by gray dots.

Furthermore, the outliers are evenly distributed to positive and negative values, which also points to a better performance of the pseudo-Voigt-based algorithm. The R_4 algorithm (Figure 2c) provides 7578 valid wind measurements with 234 outliers (3.0%), which is comparable to the pseudo-Voigt-based analysis with 50% more data points than the Lorentzian-based algorithm. The bias is (−0.25 ± 0.02) m/s and the random error is 1.60 m/s and thus, similar to the other two algorithms. The data quality control schemes and thresholds, which differ for the respective algorithms, were set such that the wind comparisons yield similar random errors. Thus, the increase in valid wind measurements can be considered as a better performance of the respective algorithm. Both the pseudo-Voigt and the R_4 algorithm perform better than the Lorentzian one, which is likely due to the better representation of the actual Fizeau fringe profile. Hence, especially for applications that require a fast computation time, the novel R_4 algorithm represents a very good alternative, since it is more than two orders of magnitude faster than the fit-based algorithms.

6. Summary

The performance of three different peak analysis algorithms – two fit-based and one intensity-ratio-based – has been investigated by means of A2D Mie channel data, where a fringe is produced by a Fizeau interferometer. Against expectations, the Fizeau fringe is shown to be best described by a Voigt spectral shape, which can be explained by an off-axis illumination of the interferometer with a divergent beam. Hence, the Voigt-fit-based algorithm performs better than the Lorentzian-fit-based one. The R_4 algorithm is demonstrated to have a similarly good performance as the Voigt algorithm, but with a much faster computation time (about a factor of 700). Therefore, it is regarded as a suitable alternative for applications where a fast computation time is needed. Moreover, the fast and accurate analysis of spectrograms from heterodyne-detection wind lidars is considered an interesting application for the R_4 method.

7. References

[1] O. Reitebuch, C. Lemmerz, E. Nagel, U. Paffrath, Y. Durand, M. Endemann, F. Fabre, and M. Chaloupy, "The airborne demonstrator for the direct-detection Doppler wind lidar ALADIN on ADM-Aeolus. Part I: instrument design and comparison to satellite instrument," J. Atmos. Oceanic Technol. **26**, 2501–2515 (2009).

[2] B. Witschas, C. Lemmerz, A. Geiß, O. Lux, U. Marksteiner, S. Rahm, O. Reitebuch, A. Schäfler, and F. Weiler, "Validation of the Aeolus L2B wind product with airborne wind lidar measurements in the polar North Atlantic region and in the tropics," Atmos. Meas. Tech. **15**, 7049–7070 (2022).

[3] B. Witschas, M. Vaughan, O. Lux, C. Lemmerz, I. Nikolaus, and O. Reitebuch, „Verification of different Fizeau fringe analysis algorithms based on airborne wind lidar data in support of ESA's Aeolus mission," Appl. Opt., **62**, 7917-7930 (2023).

[4] O. Reitebuch, D. Huber, and I. Nikolaus, "ADM-aeolus algorithm theoretical basis document (ATBD)—Level 1B products," AE.RP.DLR.L1B. 001 (2018), p. 117.

[5] B. Witschas, C. Lemmerz, O. Lux, U. Marksteiner, O. Reitebuch, F. Weiler, F. Fabre, A. Dabas, T. Flament, D. Huber, and M. Vaughan, "Spectral performance analysis of the Aeolus Fabry–Pérot and Fizeau interferometers during the first years of operation," Atmos. Meas. Tech. **15**, 1465–1489 (2022).